Nanoscale

PAPER

View Article Online
View Journal | View Issue

Cite this: *Nanoscale*, 2016, **8**, 13257

Strong electronic coupling and electron transfer in a $Ce_2@I_h$-C_{80}–H_2P electron donor acceptor conjugate†

Marc Rudolf,[a] Lai Feng,*[b,c] Zdenek Slanina,[c] Weiwei Wang,[d] Shigeru Nagase,*[d] Takeshi Akasaka*[c,e,f,g] and Dirk M. Guldi*[a]

Received 24th April 2016,
Accepted 7th June 2016

DOI: 10.1039/c6nr03324e

www.rsc.org/nanoscale

A newly designed electron donor–acceptor conjugate, namely $Ce_2@I_h$-C_{80}–H_2P consisting of an endohedral dimetallofullerene $Ce_2@I_h$-C_{80} and a free-base prophyrin (H_2P), has been synthesized and systematically investigated. Basic characterization by means of NMR spectroscopy, steady-state absorption spectroscopy, and electrochemistry points to a folded configuration with sizeable interactions between $Ce_2@I_h$-C_{80} and H_2P. Complementary DFT optimization also results in the same conclusions. Time-resolved absorption spectroscopic investigations corroborate the formation of the $(Ce_2)^{\bullet-}@I_h$-C_{80}-$(H_2P)^{\bullet+}$ radical ion pair state in non-polar as well as polar media. Overall, the modus operandi is an ultrafast through-space electron transfer enabled by the folded configuration in the ground and excited state.

Introduction

Within the context of highly efficient, cost effective artificial solar energy conversion, the exploration and testing of novel materials with unprecedented properties have been of continuous interest in recent years. Outstanding building blocks are endohedral metallofullerenes (EMF). Firstly, EMFs consist of rigid carbon cages, similar to empty fullerenes, which feature small reorganization energies in electron transfer reactions. The latter has exerted noteworthy impact on the improvement of photoinduced charge separation processes. Secondly, the electronic and photophysical properties of EMFs are tunable by changing their endohedral composition. This, on the one hand, results in strong electron acceptors that are able to outperform empty fullerenes such as C_{60} and, on the other hand, also results in strong electron donors with very low first oxidation potentials. Notably, the latter behaviour stands in stark contrast to what has been seen for empty fullerenes. Such amphoteric features render EMFs highly promising to tune the outcome of electron transfer processes as a function of solvent, endohedral composition, EMF counterpart, and so on. Thirdly, due to the presence of additional metal atoms inside the EMF, interior novel properties and phenomena arise, which might be of great value for extending the radical ion pair state lifetimes.[1–7] For instance, electron nuclear hyperfine interactions, which induce a spin-slip on transferred electrons and, thus, elongate the radical ion pair state lifetime, has been realized.[8,9] Frontier orbitals, which are encaged in the interior of EMFs like in the LUMO in $Ce_2@I_h$-C_{80} or $La_2@I_h$-C_{80}, assist in reducing the electronic coupling upon electron transfer and, therefore, increase the radical ion pair state lifetime.[10,11] Although large progress has been made in recent years towards utilizing some of EMFs outstanding properties, more research is necessary to fully understand and also explore their behaviour in electron transfer processes and to improve the performance of EMF containing electron donor–acceptor conjugates or hybrids. In recent work, $Ce_2@I_h$-C_{80} was covalently attached to a tetraphenyl zinc porphyrin (ZnP) and systematically investigated.[12] One remarkable finding of this study is a bidirectional electron transfer chemistry depending on the solvent polarity. A reductive electron transfer, namely the formation of the $(Ce_2)^{\bullet-}@I_h$-C_{80}–$(ZnP)^{\bullet+}$ radical ion pair state is observed in nonpolar media such as toluene and THF, while in polar media an oxidative electron transfer, namely formation of the $(Ce_2@I_h$-$C_{80})^{\bullet+}$–$(ZnP)^{\bullet-}$ radical ion pair state, is operative. Besides the switchable electron transfer it is one of

[a]*Department of Chemistry and Pharmacy & Interdisciplinary Center for Molecular Materials, Friedrich-Alexander-University Erlangen-Nuremberg, Erlangen 91058, Germany. E-mail: dirk.guldi@fau.de*
[b]*College of Physics, Optoelectronics and Energy, Soochow University, Suzhou 215006, China. E-mail: fenglai@suda.edu.cn*
[c]*Life Science Center of Tsukuba Advanced Research Alliance, University of Tsukuba, Ibaraki 305-8577, Japan. E-mail: akasaka@tara.tsukuba.ac.jp*
[d]*Fukui Institute for Fundamental Chemistry, Kyoto University, Kyoto 606-8103, Japan*
[e]*Foundation for Advancement of International Science, Ibaraki 305-0821, Japan*
[f]*School of Materials Science and Engineering, Huazhong University of Science and Technology, Wuhan 430074, China*
[g]*Department of Chemistry, Tokyo Gakugei University, Tokyo 184-8501, Japan*
†Electronic supplementary information (ESI) available. See DOI: 10.1039/c6nr03324e

the early milestones in photoinduced oxidative electron transfer with fullerenes in general.

Herein, we report a novel electron donor–acceptor conjugate, in which a free base tetraphenyl prophyrin (H_2P) is covalently linked to $Ce_2@I_h$-C_{80}. Incentives for the use of H_2P rather than ZnP are lower excited state energies, stronger electron acceptor strengths, weaker electron donor properties, and less ambiguous transient absorption characteristics. Full-fledged investigations have been performed to characterize this $Ce_2@I_h$-C_{80}–H_2P electron donor–acceptor conjugate in the ground and excited states.

Experimental section

Materials

All chemicals were of reagent grade and purchased from Wako. $Ce_2@I_h$-C_{80} (>99%) was prepared and isolated according to the previously reported methods. Preparative and analysis HPLC were performed on a semi preparative 5PYE column (∅10 × 100 mm, Cosmosil), a analysis 5PYE column (∅4.6 × 100 mm, Cosmosil), and a Buckyclutcher column (∅4.6 × 100 mm, Cosmosil), respectively. Toluene was used as the eluent and monitor wavelength was set to 413 nm.

Spectroscopy

All NMR spectra were recorded on a Bruker AV 500 spectrometer with a CryoProbe system, locked on deuterated solvents and referenced to the solvent peak. The 1D (^{1}H, ^{13}C and DEPT135) and 2D experiments (COSY) were performed by means of standard experimental procedures of the Bruker library. Matrix-assisted laser desorption–ionization time-of flight (MALDI-TOF) mass spectra were recorded with a Bruker BIFLEX-III mass spectrometer using 1,1,4,4-tetraphenyl-1,3-butadiene as the matrix. The measurements were performed in both positive and negative ion modes.

Electrochemistry

Differential pulse voltammetry (DPV) and cyclic voltammetry (CV) were carried out in *o*-DCB using a BAS CW-50 instrument. A conventional three-electrode cell consisting of a platinum working electrode, a platinum counter-electrode, and a saturated calomel reference electrode (SCE) was used for both measurements. 0.05 M $(n\text{-Bu})_4NPF_6$ was used as the supporting electrolyte. All potentials were recorded against a SCE reference electrode and corrected against Fc/Fc^+. DPV and CV were measured at a scan rate of 20 and 100 mV s^{-1}, respectively.

Steady-state absorption

UV-Vis spectra were recorded on a Lambda 2 spectrometer from Perkin Elmer (190 to 1100 nm; double-beam-instrument). The measurements were carried out at room temperature.

Steady-state emission

The spectra were recorded on a FluoroMax 3 fluorometer (Horiba Jobin Yvon). The measurements were carried out at room temperature.

Time-resolved absorption

Femtosecond transient absorption studies were performed with 387 and 420 nm laser pulses (1 kHz, 150 fs pulse width) from amplified Ti:sapphire laser systems (CPA-2101 and CPA-2110 from Clark-MXR, Inc.), and the laser energy was 200 nJ. The measurements were carried out at room temperature.

Computational method

The calculations were carried out using the hybrid density functional theory (DFT) at the B3LYP & D3 level[13] as implemented in the Gaussian09 software package.[14] The SDD basis set[15] with the relativistic effective core potential was employed for Ce, 3-21G basis set for C, H, O, N.[16]

Synthesis of $Ce_2@C_{80}$–H_2P (2)

Tosylhydrazone 1 (15 mg, 15 μmol) and NaOMe (2.5 mg, 45 μmol) were dissolved in a mixture of *o*-DCB and MeCN (v : v of 5 : 1, and totally 3 ml) and stirred for 40 min at 75 °C under Ar. Then, $Ce_2@C_{80}$ (3.8 mg, 3 μmol) in 5 ml *o*-DCB was added. The mixture was stirred at 75 °C for another 40 min under Ar. After cooling down, a mixture of CS_2 and acetone (v : v of 1 : 1, and totally 10 ml) containing 5 μL $CHCl_2COOH$ was added and stirred for 30 min. Then, the reaction mixture was washed with 0.5 M $NaHCO_3$ and the products were extracted using toluene. The reaction mixture in toluene was separated by HPLC (5PYE column, toluene). The second fraction is the conjugate of $Ce_2@C_{80}$–H_2P, which was further purified using a Buckyprep column. Yield: 35% based on consumed $Ce_2@C_{80}$.

^{1}H NMR (500 MHz, $C_2D_2Cl_4$, 293 K): (paramagnetic!)

δ = 10.49 (br. s, 1H), 10.05 (br. s, 1H), 9.96 (br. s, 1H), 9.80 (br. s, 1H), 9.74 (br. s, 1H), 9.55 (br. s, 1H), 9.50 (br. s, 1H), 9.40 (br. s, 1H), 9.15 (d, 1H), 9.03 (d, 1H), 8.93 (d, 1H), 8.69 (t, 1H), 8.55 (d, 1H), 8.42 (m, 2H), 8.33 (t, 1H), 8.27 (t, 1H), 8.22 (t, 1H), 7.77 (t, 1H), 7.47 (t, 1H), 7.03 (t, 1H), 6.95 (d, 1H), 6.31 (br. s, 1H), 6.12 (br. s, 1H), 4.46 (br. s, 1H), 4.38 (br. s, 1H), 4.00 (t, 1H), 3.63 (br. s, 1H), 3.58 (br. s, 1H), 2.96 (t, 1H), 2.39 (t, 1H), −0.42 (br, s, 1H), −3.19 (br. s, 1H), −3.26 (br. s, 1H), −5.15 (d, 1H), −6.43 (d, 1H), −9.66 (br. s, 1H), −10.08 (br. s, 1H), −17.62 (br. s, 1H), −18.07 (br. s, 1H).

^{13}C NMR (125 MHz, $C_2D_2Cl_4$, 293 K): (paramagnetic!)

δ = 196.84, 194.49, 192.80, 191.78, 190.24, 187.44, 186.72, 184.66, 183.77, 182.46, 178.87, 174.78, 174.15, 172.25, 171.41, 171.17, 170.86, 170.18, 169.45, 169.17, 168.97, 168.70, 166.88, 166.63, 165.45, 162.49, 158.90, 158.70, 158.64, 158.48, 158.35, 156.92, 156.85, 156.67, 156.59, 156.29, 155.35, 154.20, 154.10, 153.32, 148.90, 148.52, 148.03, 147.92, 146.95, 146.24, 145.92, 144.71, 144.65, 144.52, 144.46, 143.92, 143.66, 143.56, 142.27, 142.12, 142.05, 141.28, 137.29, 136.76, 136.62, 136.46, 136.24,

136.10, 135.89, 135.05, 134.12, 134.08, 133.15, 132.33, 130.57, 129.34, 128.86, 128.71, 128.52, 128.30, 128.21, 127.86, 127.72, 127.70, 127.31, 126.78, 126.02, 125.64, 124.44, 123.48, 123.18, 123.01, 122.87, 122.73, 122.68, 122.40, 121.64, 121.60, 119.95, 116.17, 114.74, 114.16, 113.79, 101.08, 98.74, 92.74, 87.97, 87.26 85.24, 83.28, 66.35, 62.25, 38.73, 31.43, 30.06, 27.32, 10.10, 8.53, −1.00 (spiro carbon). MS (MALDI-TOF): m/z = 2075.83 $[M + 2H]^+$; Calcd for $Ce_2C_{137}H_{44}N_4O_3$: m/z = 2073.15 (100% intensity).

Results and discussion

The synthesis of the conjugate $Ce_2@C_{80}$–H_2P (**2**) was carried out *via* a [2 + 1]-cycloaddition reaction of tosylhydrazone **1** containing a H_2P moiety (see Schemes 1, S1 and S2†). The resulting reaction mixture was separated by HPLC. It is noted that the isolated **2** has a shorter retention time on a Buckyclutcher column as compared to what has been previously reported for $Ce_2@C_{80}$–ZnP, prompting to their different compositions. **2** was further characterized by means of MALDI-TOF mass and NMR experiments. As shown in Fig. S3,† the mass spectrum of **2** shows a distinct peak at 2075.83 m/z, which is assigned to the $[2 + 2H]^{2+}$ ion. On the other hand, **2** exhibits temperature-dependent ^1H NMR spectra (see Fig. S4 and S5†), which resembles those recorded for $Ce_2@C_{80}$–ZnP.[12] All the ^1H signals were reasonably assigned based on the ^1H–^1H COSY experiments (see the ESI† for detailed assignments). In particular, the methylene and phenyl protons adjacent to the C_{80} cage shift to the up-field region beyond 0 ppm, pointing to the paramagnetic impact of the encapsulated Ce^{3+} ions. In the down-field region, the well separated signals due to porphyrin protons are found in a wide range from 11–6 ppm. This result may suggest close proximity between the endohedral Ce^{3+} ions and the porphyrin moiety, through which the individuals can efficiently interact by their magnetic dipoles.[17–19] Thus, our NMR results suggest a folded conformation for **2**, consistent with that of $Ce_2@C_{80}$–ZnP. It is likely that the longer spacer of 2-oxy-ethyl butyrate allows a close alignment of the π-electron-rich moieties $Ce_2@C_{80}$ and H_2P. Moreover, DFT-optimization also prompted to a folded conformation for **2** (see Fig. 1), in good agreement with the NMR results. The DFT-calculated LUMO (−2.73 eV) and HOMO (−4.84 eV) are distributed on the

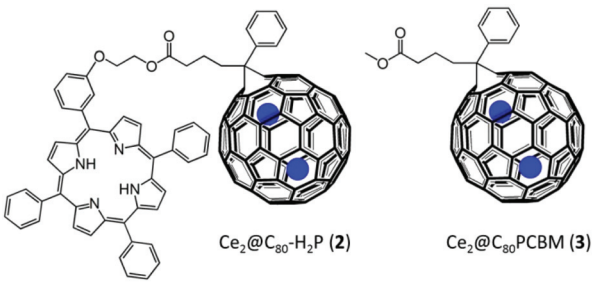

Scheme 1 Structures of electron donor–acceptor conjugate **2** and ref. 3.

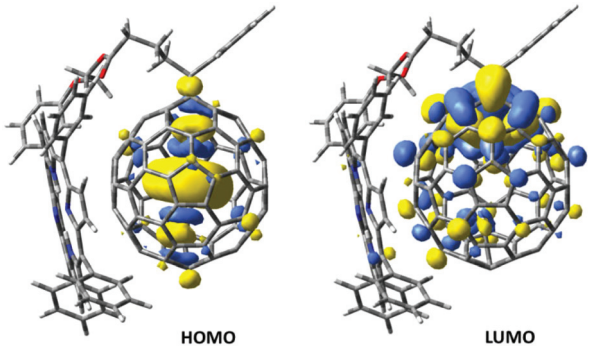

Fig. 1 DFT-optimized conformer of **2** with HOMO and LUMO distributions.

C_{80} cage and endohedral Ce_2 cluster, respectively (see Fig. 1 and S8†).

The electrochemical properties of $Ce_2@C_{80}$–H_2P (**2**) were investigated by means of differential pulse voltammetry (DPV) and cyclic voltammetry (CV) (Fig. S9–S11, see the ESI†). The redox data of **2** obtained from DPV are listed in Table 1, in comparison with those of reference compounds H_2P and **3**. As shown in DPV and CV profiles, in the anodic side, there are at least two reversible one-electron oxidations. The first and second oxidations (*i.e.*, 0.43 and 0.59 V) are assigned to the formation of the $Ce_2@C_{80}$ and H_2P radical cations, respectively. In the cathodic side, three reductions are discernable. In particular, the reversible reductions at −0.44 and −1.75 V correspond to the formation of the $Ce_2@C_{80}$ radical anion and the $Ce_2@C_{80}$ dianion/H_2P radical anion, respectively, while the third reduction at −2.07 V points to the formation of a $Ce_2@C_{80}$ trianion. Thus, both the first oxidation and reduction occur on the $Ce_2@C_{80}$ moiety, which agree well with the DFT-calculated MO distribution. Moreover, it shall be noted that the first and the second oxidations of **2** differ from the first oxidations of **3** and H_2P by 50–60 mV, respectively, indicating appreciable ground state interactions between them.

Profound electronic interactions were derived from the absorption spectra (see Fig. 2). Both Soret and Q-band transitions reveal subtle changes in $Ce_2@I_h$-C_{80}–H_2P when compared to a H_2P reference with shifts as large as 8 nm. The corresponding absorption maxima for $Ce_2@I_h$-C_{80}–H_2P and H_2P are in toluene at 419, 514, 548, 591, and 647 nm as well as 422, 520, 556, 596, and 655 nm, respectively. In addition, the extinction coefficients are impacted with values for the Soret

Table 1 Redox potentials of H_2P and $Ce_2@C_{80}$–H_2P[a]

	$^3E_{ox}$	$^2E_{ox}$	$^1E_{ox}$	$^1E_{red}$	$^2E_{red}$	$^3E_{red}$
H_2P		0.94	0.52	−1.75		
2	0.89	0.59	0.43	−0.44	−1.75[b]	−2.07
3		0.91	0.48	−0.42	−1.75	−2.23

[a] All the potentials, in volts, were measured relative to the $Fc^{0/+}$ couple by means of DPV. [b] Two-electron reduction process.

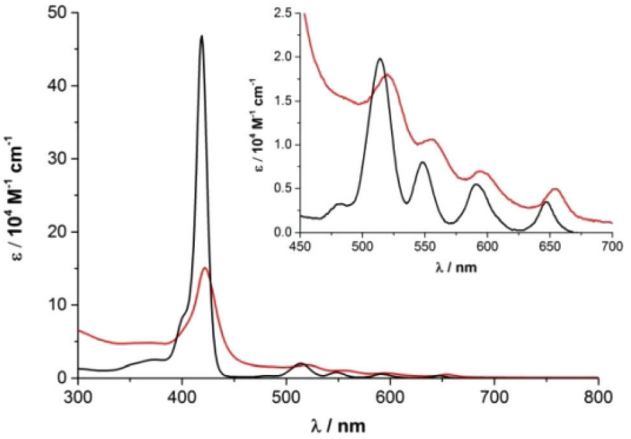

Fig. 2 UV-vis absorption spectra of $Ce_2@I_h$-C_{80}–H_2P (**2**) (red) and H_2P (black) in toluene. The inset shows a zoom in on the absorption features between 450 and 700 nm.

band absorption of 470.000 M^{-1} cm^{-1} for H_2P and of 150.000 M^{-1} cm^{-1} for $Ce_2@I_h$-C_{80}–H_2P – both in toluene.

Insights into the excited state interactions between $Ce_2@I_h$-C_{80} and H_2P came from steady-state and time-resolved fluorescence experiments. In particular, the H_2P centered fluorescence maxima at 650 and 716 nm are red shifted to 652 and 717 nm in $Ce_2@I_h$-C_{80}–H_2P and the fluorescence quantum yields are reduced from 0.11 to about 0.0011. As a matter of fact, the $Ce_2@I_h$-C_{80}–H_2P fluorescence is weakly solvent dependent with values of 0.0011 in toluene, 0.0010 in THF, and 0.0012 in benzonitrile. Fluorescence lifetimes were detected to be solvent dependent and are as short as 0.46, 0.54, and 0.79 ns in toluene, THF, and benzonitrile respectively, while the intrinsic fluorescence lifetime of H_2P is 9.8 ns.[20–23]

To further explore the excited state interactions between $Ce_2@I_h$-C_{80} and H_2P in $Ce_2@I_h$-C_{80}–H_2P, time-resolved pump probe experiments following femto- and nanosecond excitation were performed. 420 nm photoexcitation of the H_2P reference (Fig. S12, see the ESI†) leads to the instantaneous formation of transient absorption changes including maxima at 444, 538, 573, 616, 671, and 1060 nm as well as minima at 515 and 653 nm. These features, which are attributed to the singlet excited state of H_2P (1.90 eV), transform slowly with a lifetime of 10.5 ± 0.5 ns to the corresponding triplet excited state. For the latter, maxima evolve at 442, 534, 568, 623, and 780 nm, while minima evolve at 515, 549, 592, and 647 nm.

In femtosecond transient absorption measurements with $Ce_2@I_h$-C_{80}–H_2P (see Fig. 3), directly after 420 nm laser excitation, the aforementioned singlet excited state transitions of H_2P are discernible. In particular, sets of maxima at 441, 538, 573, 616, 671, and 1060 nm as well as minima at 515, 653 nm are detected. In $Ce_2@I_h$-C_{80}–H_2P, the singlet–singlet transitions decay, on the one hand, much faster than observed for the slow intersystem crossing to the H_2P triplet excited state and, on the other hand, with dynamics that are biphasic. In particular, in toluene, THF, benzonitrile, and cyclohexylisonitrile the lifetimes are 17.2 ± 0.3/408 ± 9 ps, 18.4 ± 0.4/560 ± 10 ps, 22.1 ± 20/569 ± 6 ps, and 22.1 ± 0.7/707 ± 8 ps, respectively. Notable is the lack of any appreciable transient at the end of the H_2P centered singlet excited state decay rather than the ground state. In other words, neither characteristics of the H_2P triplet excited state nor of the radical ion pair state are discernable. It seems that the $(Ce_2@I_h\text{-}C_{80})^{\bullet-}$–$(H_2P)^{\bullet+}$ radical ion pair, once formed, decays ultrafast and does not build up a noticeable concentration of $(Ce_2@I_h\text{-}C_{80})^{\bullet-}$–$(H_2P)^{\bullet+}$ to be spectroscopically detectable. A rationale for the short-lived component would be a partial charge transfer, namely $(Ce_2@I_h\text{-}C_{80})^{\delta-}$–$(H_2P)^{\delta+}$, that opens up another spectroscopically silent decay channel *via* the $(Ce_2@I_h\text{-}C_{80})^{\bullet-}$–$(H_2P)^{\bullet+}$ charge separated state. Unfortunately, there is no direct spectroscopic evidence for either $(Ce_2@I_h\text{-}C_{80})^{\delta-}$–$(H_2P)^{\delta+}$ or $(Ce_2@I_h\text{-}C_{80})^{\bullet-}$–$(H_2P)^{\bullet+}$, however, solvent dependent kinetics in our transient absorption studies support our suggested mechanism.

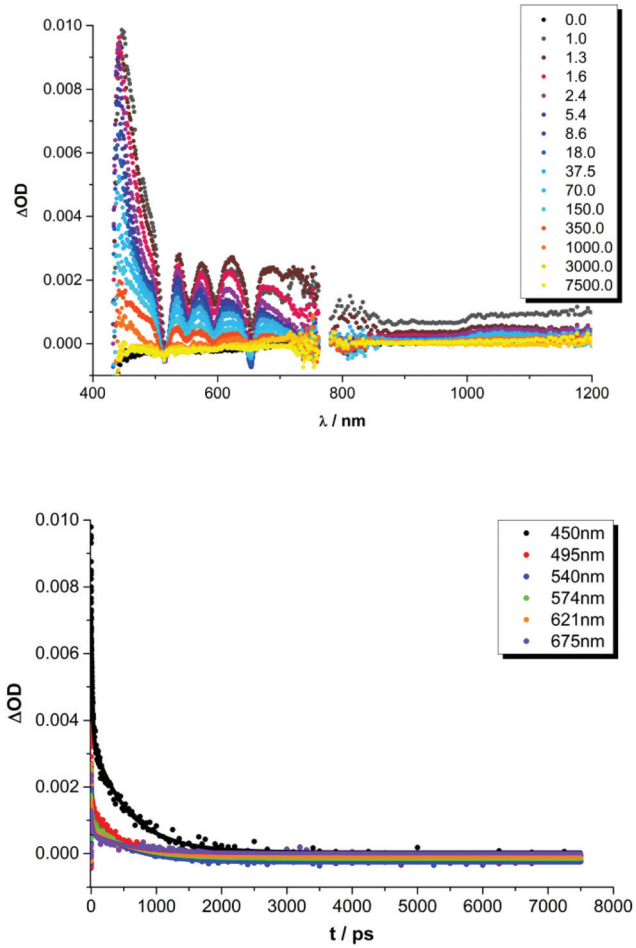

Fig. 3 (Top) Differential absorption spectra (visible and near infrared) obtained upon femtosecond flash photolysis (420 nm) of $Ce_2@I_h$-C_{80}–H_2P (10^{-5} M) in argon-saturated THF with several time delays between 0 and 7500 ps at room temperature. (Bottom) Time-absorption profiles of the spectra shown above at 450, 495, 540, 574, 621, and 675 nm monitoring the excited state decay.

From the solvent dependency of the H_2P singlet excited state deactivation we infer an electron transfer rather than energy transfer. In a recent study on $Ce_2@I_h$-C_{80}–ZnP,[12] a shift from a reductive electron transfer to afford $(Ce_2@C_{80})^{\bullet-}$–$(ZnP)^{\bullet+}$ to an oxidative electron transfer to yield $(Ce_2@C_{80})^{\bullet+}$–$(ZnP)^{\bullet-}$ was noted when nonpolar toluene and THF were replaced by polar benzonitrile and DMF, respectively. In the current study on $Ce_2@C_{80}$–H_2P, lowering the reduction potential of the porphyrin by 0.2 eV should enable the oxidative electron transfer even in nonpolar toluene and THF. It is, however, important to note that the H_2P singlet excited state (1.90 eV) is 0.2 eV lower in energy than the ZnP singlet excited state (2.10 eV) and, thus, provides less thermodynamic driving force. The $(Ce_2@C_{80})^{\bullet-}$–$(H_2P)^{\bullet+}$ charge separated state is higher in energy compared to the $(Ce_2@C_{80})^{\bullet-}$–$(ZnP)^{\bullet+}$ radical ion pair by approximately 0.2 eV (see Fig. 4), since H_2P is harder to oxidize than ZnP. In such a scenario the thermodynamic driving force for the $(Ce_2@C_{80})^{\bullet-}$–$(H_2P)^{\bullet+}$ radical ion pair state formation from the H_2P singlet excited state is reduced by 0.4 eV with respect to the corresponding $(Ce_2@C_{80})^{\bullet-}$–$(ZnP)^{\bullet+}$ formation from the ZnP singlet excited state. The resulting change in exergonicity renders the $(Ce_2@C_{80})^{\bullet-}$–$(H_2P)^{\bullet+}$ formation more favorable, since the charge separated state is closer to the top of the Marcus parabola. In particular, the solvent corrected free energy changes ($-\Delta G^0$) for a reductive electron transfer to yield $(Ce_2@C_{80})^{\bullet-}$–$(H_2P)^{\bullet+}$, are −0.80 eV in toluene, −1.06 eV in THF, −1.14 eV in benzonitrile, and −1.15 eV in DMF. On the other hand, the oxidative electron transfer, which affords the $(Ce_2@C_{80})^{\bullet+}$–$(H_2P)^{\bullet-}$ radical ion pair state formation, is either endergonic with $-\Delta G^0$ of +0.34, +0.09, and +0.01 eV in toluene, THF, and benzonitrile, respectively or isoenergetic with $-\Delta G^0$ of 0.00 eV in DMF with respect to the H_2P singlet excited state. In other words, there it lacks an appreciable thermodynamic driving force. In fact, a Weller type analysis on the basis of the Born dielectric continuum model[24] reveals radical ion pair energies of 2.24, 1.99, 1.91, and 1.90 eV in toluene, THF, benzonitrile, and DMF, respectively. Therefore, we conclude that the reductive electron transfer to create $(Ce_2@C_{80})^{\bullet-}$–$(H_2P)^{\bullet+}$, is favored over the oxidative electron transfer, which involves the formation of $(Ce_2@C_{80})^{\bullet+}$–$(H_2P)^{\bullet-}$, in $Ce_2@I_h$-C_{80}–H_2P in polar as well as non-polar solvents.

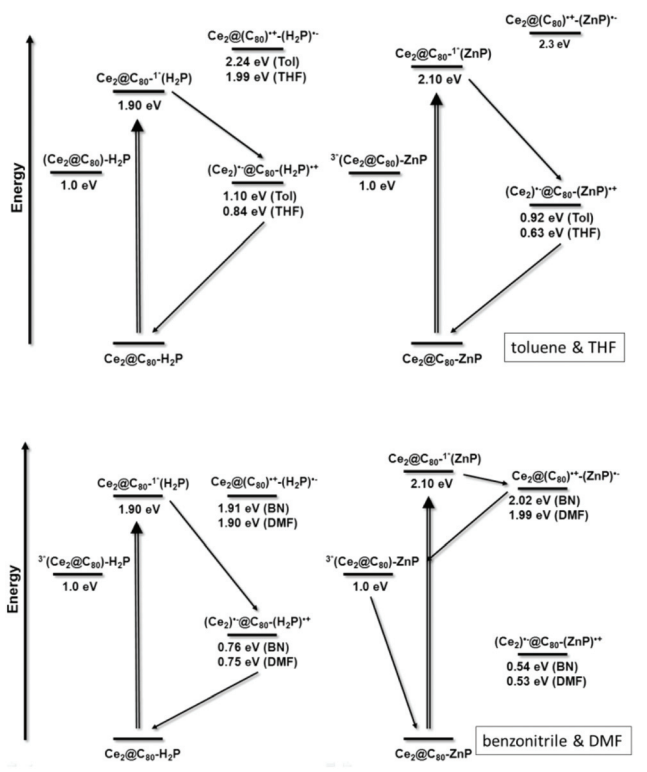

Fig. 4 Energy diagram for $Ce_2@I_h$-C_{80}–H_2P on the left and for $Ce_2@I_h$-C_{80}–ZnP on the right illustrating the different excited state deactivation pathways that lead in toluene and THF (top) and benzonitrile and DMF (bottom) to different charge transfer products. Values for $Ce_2@C_{80}$–ZnP were taken from the literature.[12]

Conclusions

In conclusion, we have synthesized a covalently linked $Ce_2@C_{80}$–H_2P electron donor–acceptor conjugate. NMR experiments suggest a folded conformation, in which $Ce_2@C_{80}$ and H_2P tightly interact. Photophysical measurements demonstrate that, in a nutshell, a reductive electron transfer is operative in the $Ce_2@C_{80}$–H_2P electron donor–acceptor conjugate to afford the corresponding $(Ce_2)^{\bullet-}@I_h$-C_{80}–$(H_2P)^{\bullet+}$ radical ion pair state in non-polar as well as polar media. Hereby, the charge separation is postulated to be the rate determining step. Implicit is that the charge recombination is faster and, in turn, is undetectable in our time-resolved laser studies.

Acknowledgements

This work is financially supported by the Deutsche Forschungsgemeinschaft (GU 517/14-1), and the NSFC (51372158), the Jiangsu Specially Appointed Professor Program (SR10800113), the Project for Jiangsu Scientific and Technological Innovation Team (2013).

Notes and references

1 H. Shinohara, *Rep. Prog. Phys.*, 2000, **63**, 843–892.
2 H. Shinohara, in *Fullerenes: Chemistry, Physics, and Technology*, ed. K. M. Kadish and R. S. Ruoff, Wiley, New York, 2000, pp. 357–393.
3 T. Akasaka and S. Nagase, *Endofullerenes: A New Family of Carbon Clusters*, Kluwer, Dordrecht, The Netherlands, 2002.
4 L. Feng, T. Akasaka and S. Nagase, in *Carbon Nanotubes and Related Structures*, ed. D. M. Guldi and N. Martín, Wiley-VCH, Weinheim, 2009.
5 M. Rudolf, S. Wolfrum, D. M. Guldi, L. Feng, T. Tsuchiya, T. Akasaka and L. Echegoyen, *Chem. – Eur. J.*, 2012, **18**, 5136–5148.

6 M. Lederer, M. Rudolf, M. Wolf, D. M. Guldi, S. Zhao, X. Lu and L. Feng, in *Endohedral Metallofullerenes: Basics and Applications*, ed. X. Lu, L. Echegoyen, A. L. Balch, S. Nagase and T. Akasaka, CRC Press, Boca Raton, 2015, pp. 211–254.
7 D. Gust, T. A. Moore and A. L. Moore, *Acc. Chem. Res.*, 2009, **42**, 1890–1898.
8 L. Feng, M. Rudolf, S. Wolfrum, A. Troeger, Z. Slanina, T. Akasaka, S. Nagase, N. Martín, T. Ameri, C. J. Brabec and D. M. Guldi, *J. Am. Chem. Soc.*, 2012, **134**, 12190–12197.
9 M. Rudolf, L. Feng, Z. Slanina, T. Akasaka, S. Nagase and D. M. Guldi, *J. Am. Chem. Soc.*, 2013, **135**, 11165–11174.
10 Y. Iiduka, O. Ikenaga, A. Sakuraba, T. Wakahara, T. Tsuchiya, Y. Maeda, T. Nakahodo, T. Akasaka, M. Kako, N. Mizorogi and S. Nagase, *J. Am. Chem. Soc.*, 2005, **127**, 9956–9957.
11 T. Tsuchiya, M. Rudolf, S. Wolfrum, S. G. Radhakrishnan, R. Aoyama, Y. Yokosawa, A. Oshima, T. Akasaka, S. Nagase and D. M. Guldi, *Chem. – Eur. J.*, 2013, **19**, 558–565.
12 D. M. Guldi, L. Feng, S. G. Radhakrishnan, H. Nikawa, M. Yamada, N. Mizorogi, T. Tsuchiya, T. Akasaka, S. Nagase, M. Ángeles Herranz and N. Martín, *J. Am. Chem. Soc.*, 2010, **132**, 9078–9086.
13 S. Grimme, J. Antony, S. Ehrlich and H. Krieg, *J. Chem. Phys.*, 2010, **132**, 154104.
14 M. J. Frisch, G. W. Trucks, H. B. Schlegel, G. E. Scuseria, M. A. Robb, J. R. Cheeseman, G. Scalmani, V. Barone, B. Mennucci, G. A. Petersson, H. Nakatsuji, M. Caricato, X. Li, H. P. Hratchian, A. F. Izmaylov, J. Bloino, G. Zheng, J. L. Sonnenberg, M. Hada, M. Ehara, K. Toyota, R. Fukuda, J. Hasegawa, M. Ishida, T. Nakajima, Y. Honda, O. Kitao, H. Nakai, T. Vreven, J. A. Montgomery, Jr., J. E. Peralta, F. Ogliaro, M. Bearpark, J. J. Heyd, E. Brothers, K. N. Kudin, V. N. Staroverov, R. Kobayashi, J. Normand, K. Raghavachari, A. Rendell, J. C. Burant, S. S. Iyengar, J. Tomasi, M. Cossi, N. Rega, J. M. Millam, M. Klene, J. E. Knox, J. B. Cross, V. Bakken, C. Adamo, J. Jaramillo, R. Gomperts, R. E. Stratmann, O. Yazyev, A. J. Austin, R. Cammi, C. Pomelli, J. W. Ochterski, R. L. Martin, K. Morokuma, V. G. Zakrzewski, G. A. Voth, P. Salvador, J. J. Dannenberg, S. Dapprich, A. D. Daniels, O. Farkas, J. B. Foresman, J. V. Ortiz, J. Cioslowski and D. J. Fox, *Gaussian 09, Revision D.01*, Gaussian, Inc., Wallingford, CT, 2009.
15 X. Cao and M. Dolg, *THEOCHEM*, 2002, **581**, 139–147.
16 A. D. Becke, *J. Chem. Phys.*, 1993, **98**, 5648–5652.
17 T. Wakahara, J.-I. Kobayashi, M. Yamada, Y. Maeda, T. Tsuchiya, M. Okamura, T. Akasaka, M. Waelchi, K. Kobayashi, S. Nagase, K. Kato, M. Kako, K. Yamamoto and K. M. Kardish, *J. Am. Chem. Soc.*, 2004, **126**, 4883–4887.
18 M. Yamada, T. Wakahara, T. Nakahodo, T. Tsuchiya, Y. Maeda, T. Akasaka, K. Yoza, E. Horn, N. Mizorogi and S. Nagase, *J. Am. Chem. Soc.*, 2006, **128**, 1402–1403.
19 M. Yamada, N. Mizorogi, T. Tsuchiya, T. Akasaka and S. Nagase, *Chem. – Eur. J.*, 2009, **15**, 9486–9493.
20 D. Kuciauskas, S. Lin, G. R. Seely, A. L. Moore, T. A. Moore, D. Gust, T. Drovetskaya, C. A. Reed and P. D. W. Boyd, *J. Phys. Chem.*, 1996, **100**, 15926–15932.
21 W. A. Lee, M. Grätzel and K. Kalyanasundaram, *Chem. Phys. Lett.*, 1984, **107**, 308–313.
22 K. Tamaki, H. Imahori, Y. Sakata, Y. Nishimura and I. Yamazaki, *Chem. Commun.*, 1999, 625–626.
23 S. Schlundt, G. Kuzmanich, F. Spänig, G. de Miguel ojas, C. Kovacs, M. A. Garcia-Garibay, D. M. Guldi and A. Hirsch, *Chem. – Eur. J.*, 2009, **15**, 12223–12233.
24 A. Weller, *Z. Phys. Chem.*, 1982, **133**, 93.

